Capillary Migration of Large Confined drops in Super-hydrophobic Wedges

Notes

Logan Torres

April 2017

When confined within an interior corner, drops and bubbles migrate to regions of minimum energy by the combined effects of surface tension, surface wetting, and corner geometry. Such capillary phenomena are exploited for passive phase separation operations in micro-fluidic devices on earth and macro- fluidic devices aboard spacecraft. Our study focuses on the migration of large inertial-capillary drops confined between two planar super-hydrophobic surfaces. In our experiments, the near weightless environment of a drop tower produces Bo $\ll 1$ for drop volumes O(10mL) with migration velocities up to 10 cm/s. We observe transient behavior as a function of drop volume, wedge angle, initial confinement, and fluid properties including contact angle. We then further demonstrate how the experiment method may be employed as a large horizontal quiescent droplet generator for studies ranging from inertial non-wetting moving contact line investigations to large geyser-free horizontal drop impacts.

Introduction

Devices in aerospace and micro-tech fluid management are seeing increasing integration of passive control mechanisms, one of which is in the form of capillary fluidics. Capillary phenomena become prominent as the non-dimensional parameter Bo becomes small $O(<<1)$, as is often the case in small length scale systems or in micro-gravity environments. In such regimes, pressure variations proportional to the mean curvature and surface tension given by the Laplace Equation $\Delta P = \sigma\mathcal{K}$ are present and can lead to sufficiently large pressure gradients when either the mean curvature $\mathcal{K}$ or surface tension value σ varies across the fluid body. Introduction of surfactants and temperature gradients are often employed to vary the surface tension of a liquid while confinement geometry and wetting conditions are used to change the curvature of the liquid interface.

Creation and/or control of volumes of fluids such a droplets and bubbles are often the focus of said research. Immersed liquids in lab-on-a-chip devices, which are driven through micro-channels, exploit the enhanced effects of surface tension to generate precise volumes of reactants for controlled reactions and prodction of drugs mixtures. Dangla *et al.* [1] proposed a passive confinement gradient for micro-fluidic droplet

generation by exploiting the hydrodynamic instability of a immersed flow encountering a step change in a channel which is accompanied with nozzled upper and lower channel walls. Their research demonstrated the independence of droplet volume on the channel flow rate or fluid properties such that only geometrical changes were required for change in volume, a key benefit over other methods which are highly flow and fluid property dependent. For space systems, the contamination of fluid systems by bubbles can pose a dangerous challenge, as bouyancy effects are absent. Recently, methods for bubble coelences or removal from such fluids systems have been demonstrated by Jenson *et al.* [2] through passive capillary migration of bubbles in conduits. This simple in design but complex in analysis system poses an advantage to high pressure system alternatives for its passive, reliable nature which is desired for long duration space missions.

Apart from direct engineering investigations, analytical models to describe the dyanmic of droplets moving and orienting in wedge like geometries poses an interesting problem to solve. Reyssat [3] pursued an analytical model for wetting droplets migrating into a wedge as well as non-wetting bubbles migrating out. Under a visco-capillary dominate regime, droplets and bubbles exhibit equivilent power law transient dyanmics as they migrate from their intial location. For droplets with contact angles satisfying the Concus-finn wetting condition [4], there is bulk migration of the droplet towards the wedge vertex where, once in contact, the volume will spread indefinitely. For contact angles greater the Concus-Finn wetting condition, the inverse problem is found which is also accompanied with a spherical equilibrium shape for drops and bubbles. Xu *et al.* [5] investigated the the equilibrium shapes for wedges oriented vertically with respect to gravity with controlled wettability by electro-wettting.

Investigations

Experimental

Droplet confinement experiments were conducted inside the Dryden Drop Tower, during which they experienced gravity on the order of $10^{-4}g$ for a time of $t_d = 2.1$s. Due to this near weightless environment, water volumes of up to $O(10^3)$mL will satisfy the relevant parameter $Bo << 1$. Confinement experiments were conducted with volumes up to 15mL. Super-hydrophobic surfaces exhibiting static contact angles $\theta_s = 151 \pm 5^\circ$ were accrued from fine-grit sandpaper coated with an aerosol PTFE spray. Flat, arylic plates 3.2-6.4mm in thickness supplied a rigid surface upon which to mount the super-hydrophobic substrates. Two experimental setup were used during experiments: a wedge test cell referred to as a WTC or a wedge apparatus referred to as WA. Depictions of each is shown in Fig. ##. The test cell or apparatus is mounted to a platform referred to as a test rig, which is designed for use in the drop tower. The test rig contains a diffuse LED light panel and high definition, commercial video camera [6] to capture images of the experiment at frame rates up to 120fps during free-fall. The test rig is assembled such that the camera is perpendicular to a plane that

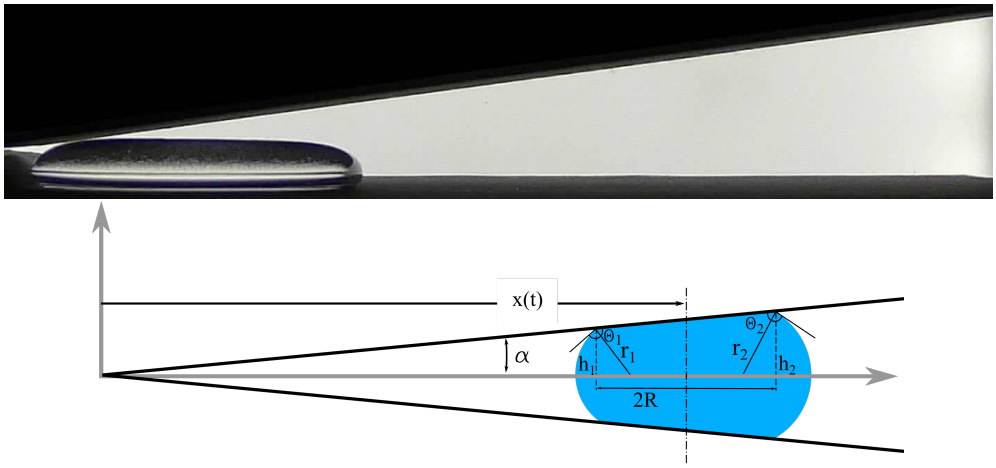

Figure 1

intersects the wedge at it's half width in which the droplet migrates along. Data is acquired from the series of images captured during free-fall, and later reduced using image processing software [7].

Experiments start with the volume of fluid resting under gravity on a horizontal, hydrophobic surface. A similar surface is held above and just slightly in contact with the droplet as depicted by Fig. (1). Following the release of the experiment and a short re-orientation period, the trailing and leading edge menisci initial locations, identified in Fig. 2 as X_{to} and X_{lo} respectively, are measured by the known geometry of the system. The droplet location is then tracked using image processing software (Spotlight-16) by the trailing edge X_t.

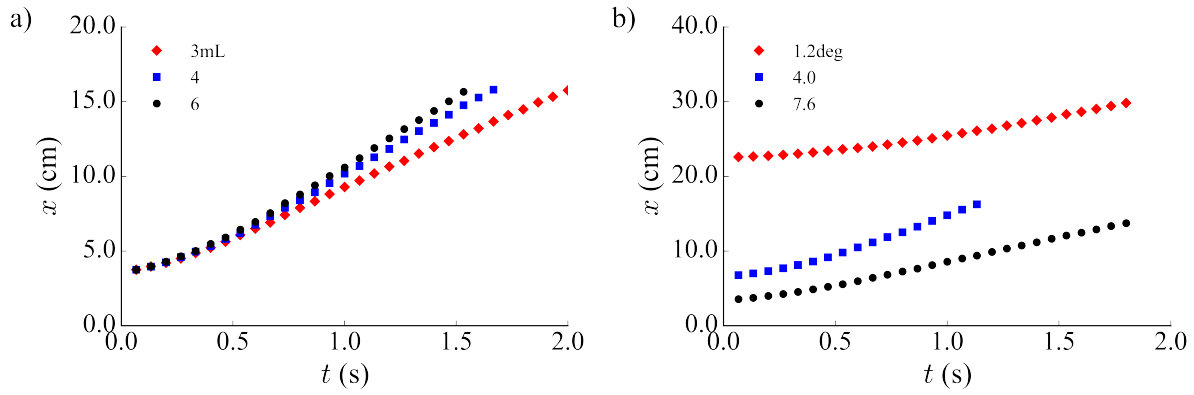

Figure 2: a) 7.6° b) 3mL

Analytical

Pressure

For the geometry above, we look to find an expression for the pressure difference encountered across the inside of the droplet. To reduce complexity, we find expressions for the radii of curvature for the advancing r_2 and receding r_1 menisci in terms of the corner half heights h_2 and h_1, given by $\frac{h_1}{r_1} = -\cos(\theta_1 - \alpha)$ and $\frac{h_2}{r_2} = -\cos(\theta_2 + \alpha)$ where α is the coner half angle and θ_1 and θ_2 are the contact angles for the receding and advancing edges respectively. We note that θ_1 and θ_2 are bounded by $\theta_{advancing}$ and $\theta_{receding}$. Laplace's Law may be used to find the pressure difference across the convex interfaces 1 and 2 and are given by

$$P_{io} - P_i = -\sigma\Big(\frac{1}{r_i} + \frac{1}{r_{io}}\Big) \tag{1}$$

where P_{io} is the ambient pressure, P_i is the internal pressure of the droplet, r_i is the radius of the interface, and r_{io} is the out of plain radius of curvature, all evaluated at location i. Note the negative value in front of the fraction accounts for the convex profile of each menisci. Evaluating Eq. (1) at both interfaces identified in Fig. (3) and taking the difference noting that the external pressure field and out of plane radius of curvature is the same for both interfaces, we find the pressure difference between interface 2 and 1 as follows

$$P_1 - P_2 = \sigma\Big(\frac{\cos(\theta_2 + \alpha)}{h_2} - \frac{\cos(\theta_1 + \alpha)}{h_1}\Big) \tag{2}$$

Taking note the relationship between the half widths of each interface we find that $h_1 < h_2$. Furthermore the contact angle for each edge is greater than $\pi/2$, $\theta_{1,2} \gg \pi/2$, and therefore $\cos(\theta_{1,2} \pm \alpha) < 0$. We now resolve that the pressure inside interface 1 is greater than the pressure inside face 2, $P_1 - P_2 > 0$, resulting in spontaneous migration away from the apex.

A second pressure term is present and acts perpendicular to the top and bottom surfaces with a contribution proportional to the sin of the half angle in the direction of interface 2. Averaging the pressure inside both mensici, $P_{ave} = P_o - \frac{\sigma}{2}\Big(\frac{\cos(\theta_2+\alpha)}{h_2} + \frac{\cos(\theta_1+\alpha)}{h_1}\Big)$, and evaluating a force balance on each surface we get

$$P_{ave} - P_o = \frac{\sigma}{2}\Big(\frac{\cos(\theta_2 + \alpha)}{h_2} + \frac{\cos(\theta_1 + \alpha)}{h_1}\Big)$$

Scaling

The drop jump velocity is estimated analytically in the large puddle volume limit by assuming a sufficiently non-wetting puddle of cylindrical disk shape with radius R_1 and height H. We ignore viscous losses due to shear, roll-up, receding contact line motion, and air drag. We assume the drop ultimately achieves a spherical configuration of radius $R_2 = R_d$ and that no satellite drops are formed. Non-spherical distortions

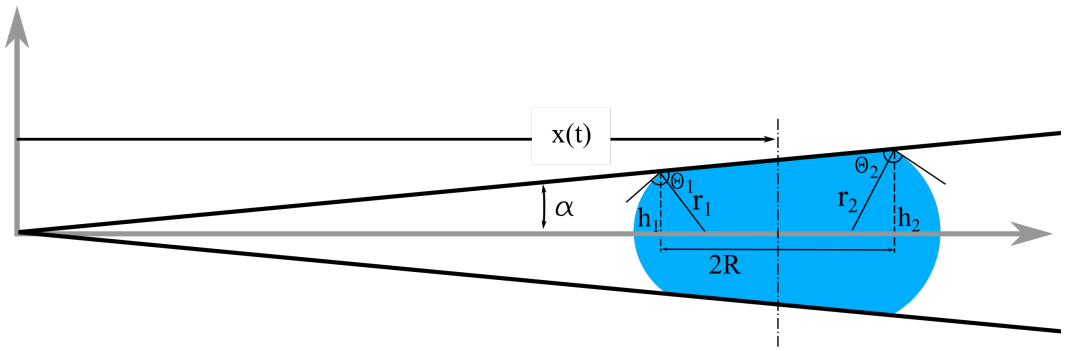

Figure 3

of the drop during the jump are eventually damped by viscous forces which are also ignored. These idealized initial and final states are depicted schematically in Fig. 11b and c.

Using the notation of Fig. 11b and c, the surface energies for liquid-solid (ls), gas-liquid (gl), and solid- gas (sg) for cylindrical disk and spherical shapes are $SE_1 = [(\sigma A)_{ls} + (\sigma A)_{gl} + (\sigma A)_{sg}]_1$ and $SE_2 = [(\sigma A)_{gl} + (\sigma A)_{sg}]_2$, respectively. From Youngs equation we have $\sigma_{sl} - \sigma_{sg} = \sigma_{gl} cos\theta$, where $R_1 = R_p = (V_d/\pi H)^{1/2}$, $R_2 = R_d = (3V_d/4\pi)^{1/3}$, and $H \approx 2(\sigma/\rho g)^{1/2}$. From $KE = SE_1 - SE_2$ we find

$$U = \frac{\sigma g}{\rho}^{1/4}\Big[-2\cos\theta + 2\big(\frac{\pi H^3}{V_d}\big)^{1/2} - 6^{2/3}\big(\frac{\pi H^3}{V_d}\big)^{1/3}\Big]^{1/2} \equiv \Big(\frac{\sigma \tilde{W} e_j}{\rho R_d}\Big)^{1/2} \tag{3}$$

In the large puddle limit $(\pi H^3/V_d)^{1/3} \ll 1$, and for $\pi/2 \leq \theta \leq \pi$, eq. (5) reduces to

$$U = \Big(\frac{\sigma g}{\rho}\Big)^{1/4}\big(-2\cos\theta\big)^{1/2} \tag{4}$$

when $\theta = \pi$ the maximum puddle jump limit is found to be

$$\tilde{U} \approx \Big(\frac{4\sigma g}{\rho}\Big)^{1/4} \tag{5}$$

Identifying an inscribed location $L_R \approx R/\sin\alpha$ where $R = R_{sphere} = (3V_d/4\pi)^{1/3}$ and initial confined location $x_o = H/2\sin\alpha$ where $H \approx 2(\sigma/\rho g)^{1/2}$ along with the the scale velocity $\tilde{U}$, we find the ejection time $t_{jw} = \frac{L_r - x_o}{U} \approx \frac{\frac{3V}{4\pi}^{1/3} - \frac{H}{2}}{\tilde{U}\sin\alpha}$. Expanding velocity term we find

$$t_{jw} = \frac{\big(\frac{3V}{4\pi}\big)^{1/3}\big(\frac{\rho}{\sigma g}\big)^{1/4}}{\sin\alpha}\frac{\Big[1 - 6^{1/3}(\frac{\pi H^3}{V})^{1/3}\Big]}{\Big[-2\cos\theta + 2\frac{\pi H^3}{V}^{1/2} - 6^{2/3}(\frac{\pi H^3}{V})^{1/3}\Big]} \tag{6}$$

Under the small volume approximation $\frac{\pi H^3}{V}^{1/3} \ll 1$

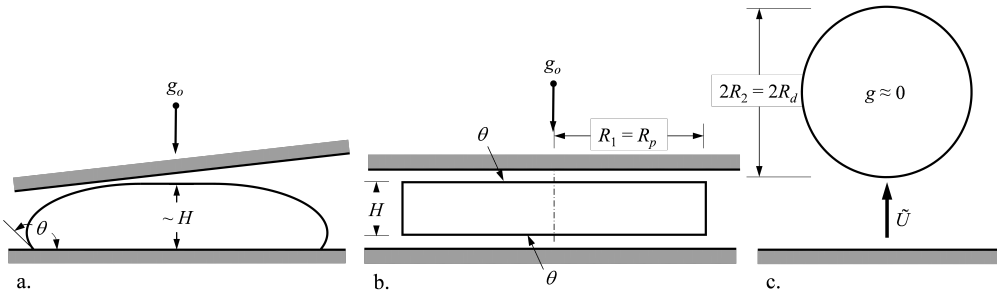

Figure 4: Given

$$t_{jw} = \Big(\frac{3V}{4\pi}\Big)^{1/3}\Big(\frac{\rho}{\sigma g}\Big)^{1/4}\frac{1}{-2\cos\theta\sin\alpha} \tag{7}$$

Volume

The wedge droplet can be constructed from two geometries: (1) an internal sliced column and (2) a variable internal radius torus. Volume (1) is easily solved in terms of its diameter, $2R$, which is represented by the perpendicular distance between h_1 and h_2 (see Fig. 1) given by

$$V_{inner} = \pi R^2(h_1 + h_2) \tag{8}$$

Volume (2) is more challenging. The complexity of the problem is resolved by taking an average of two outer-half torii of radius h_1 and h_2. The area of a circular segment is given by

$$A_{seg} = r^2\Big(\frac{2\beta_{1,2} - \sin 2\beta_{1,2}}{2}\Big) \tag{9}$$

where $\beta_{1,2} = \theta_{1,2} \pm \alpha - \pi/2$. This area is revolved around the droplet average center indentified in Fig. (1) to compute the volume.

$$V_{seg} = 2\pi(R + \Delta r)r^2\Big(\frac{2\beta_{1,2} - \sin 2\beta_{1,2}}{2}\Big) \tag{10}$$

where $\Delta r = r\frac{4\sin^3\beta}{6\beta - 3\sin 2\beta} - r\cos\beta$ is the distance from the segment planar face to the segment centroid.

$$V_{seg} = 2\pi Rr^2\Big(\frac{2\beta - \sin 2\beta}{2}\Big) + 2\pi r^3\Big(\frac{2\beta - \sin 2\beta}{2}\Big)\frac{4\sin^3\beta}{6\beta - 3\sin 2\beta} - 2\pi r^3\Big(\frac{2\beta_{1,2} - \sin 2\beta_{1,2}}{2}\Big)\cos\beta \tag{11}$$

$$V_{seg} = 2\pi\Big(Rr^2 - r^3\cos\beta\Big)\Big(\frac{2\beta - \sin 2\beta}{2}\Big) + 2\pi r^3\Big(\frac{4\sin^3\beta}{6}\Big) \tag{12}$$

Using the relationships of eq. (1) and (2) along with $\beta = \beta(\theta, \alpha)$ from eq. (7) $r = h/\sin\beta$ we substitue and resolve

$$V_{seg} = \frac{4\pi}{3}h^3 + 2\pi\Big(Rh^2\sin\beta - h^3\cos\beta\Big)\Big(\frac{2\beta - \sin 2\beta}{2\sin^3\beta}\Big) \tag{13}$$

which matches a test drawing of a segmented toriod in SolidWorks.

We want to determine the pressure at each location of the droplet as a function of time x(t).

β is a function of the contact angle and the corner half angle, which we assume is different the front and back meniscii. Therefore, to find the estimated volume of the outter toroid, we average eq. (11) using the given heights and βs for each menscii respectively.

$$\phi = \frac{2\beta - \sin 2\beta}{2\sin^3\beta}$$

$$V_{seg_{ave}} = \frac{2\pi}{3}(h_1^2 + h_2^2) + \pi\Big(R\big(h_1^2\sin\beta_1\phi_1 + h_2^2\sin\beta_2\phi_2\big) - \big(h_1^3\cos\beta_1\ \big)\Big) \tag{14}$$

Appendix

$$\frac{h_1}{r_1} = \sin(\theta_1 - \alpha - \frac{\pi}{2}) = -\cos(\theta_1 - \alpha) \tag{15}$$

$$\frac{h_2}{r_2} = sin(\theta_2 + \alpha - \frac{\pi}{2}) = -\cos(\theta_2 + \alpha \tag{16}$$

$$P_o - P_1 = -\sigma\Big(\frac{1}{r_1} + \frac{1}{r_3}\Big) = \sigma\Big(\frac{\cos(\theta_1 - \alpha)}{h_1} - \frac{1}{r_3}\Big) \tag{17}$$

$$P_o - P_2 = -\sigma\Big(\frac{1}{r_2} + \frac{1}{r_3}\Big) = \sigma\Big(\frac{\cos(\theta_2 + \alpha)}{h_2} - \frac{1}{r_3}\Big) \tag{18}$$

$$(P_o - P_2) - (P_o - P_1) = P_1 - P_2 = \frac{\sigma\cos(\theta_2 + \alpha)}{h_2} - \frac{\sigma\cos(\theta_1 + \alpha)}{h_1} \tag{19}$$

$$P_1 - P_2 = \sigma\Big(\frac{\cos(\theta_2 + \alpha)}{h_2} - \frac{\cos(\theta_1 + \alpha)}{h_1}\Big) \tag{20}$$

References

[1] R. Dangla, S. C. Kayi, and C. N. Baroud, "Droplet microfluidics driven by gradients of confinement," *Proceedings of the National Academy of Sciences*, vol. 110, no. 3, pp. 853–858, 2013.

[2] R. M. Jenson, A. P. Wollman, M. M. Weislogel, L. Sharp, R. Green, P. J. Canfield, J. Klatte, and M. E. Dreyer, "Passive phase separation of microgravity bubbly flows using conduit geometry," *International Journal of Multiphase Flow*, 2014.

[3] E. Reyssat, "Drops and bubbles in wedges," *J. Fluid Mech*, vol. 748, pp. 641–662, 2014.

[4] P. Concus and R. Finn, "Discontinuous behavior of liquids between parallel and tilted plates," *Phys. Fluids*, vol. 10, no. 1998, pp. 39–43, 1998.

[5] W. Xu, Z. Lan, B. Peng, R. Wen, Y. Chen, and X. Ma, "Directional Movement of Droplets in Grooves: Suspended or Immersed?," *Scientific reports*, vol. 6, p. 18836, 2016.

[6] Panasonic Corporation of North America, "Basic Owner's Manual HC-V770 HC-WX970," 2014.

[7] R. Kilmek and T. Wright, "Spotlight-16," 2004.